# Mechanism of RNase $T_1$: concerted triester-like phosphoryl transfer via a catalytic three-centered hydrogen bond

Stefan Loverix [1], Anna Winqvist [2], Roger Strömberg [3] and Jan Steyaert [1]

**Background**: The microscopic events of ribonuclease (RNase) catalyzed phosphoryl transfer reactions are still a matter of debate in which the contenders adhere to either the classical concerted acid–base mechanism or a more sequential triester-like mechanism. In the case of RNase A, small thio-effects of the nonbridging oxygens have been invoked in favor of the classical mechanism. However, the RNase $T_1$ catalyzed transphosphorylation of phosphorothioate RNA is highly stereoselective. $R_P$ thio-substituted RNA is depolymerized 60 000 times faster than $S_P$ thio-substituted RNA by this enzyme, whereas the uncatalyzed cleavage of both substrates occurs at comparable rates. We combined site-directed mutagenesis in the RNase active site and stereospecific thio-substitution of an RNA substrate to probe the intermolecular interactions of the enzyme with the nonbridging *pro*-$S_P$ oxygen that bring about this stereoselectivity of RNase $T_1$.

**Results**: Thio-substitution of the nonbridging *pro*-$S_P$ oxygen in the substrate afflicts chemical turnover but not ground state binding whereas thio-substitution of the nonbridging *pro*-$R_P$ oxygen does not affect the kinetics of RNase $T_1$. Site-directed mutagenesis of the catalytic base Glu58 impairs the enzyme's ability to discriminate both phosphorothioate diastereomers. Glu58Ala RNase $T_1$ cleaves $R_P$ and $S_P$ phosphorothioate RNA with similar rates. The dependence of the *pro*-$S_P$ thio-effect on the presence of the Glu58 carboxylate evidences a strong rate-limiting interaction between the nonbridging *pro*-$S_P$ oxygen and the catalytic base Glu58 in the wild type enzyme.

**Conclusions**: Based on these results, we put forward a new triester-like mechanism for the RNase $T_1$ catalyzed reaction that involves a three-centered hydrogen bond between the 2′-OH group, the nonbridging *pro*-$S_P$ oxygen and one of the carboxylate oxygens of Glu58. This interaction allows nucleophilic attack on an activated phosphate to occur simultaneously with general base catalysis, ensuring concerted phosphoryl transfer via a triester-like mechanism.

[1]Dienst Ultrastructuur, Vlaams Interuniversitair Instituut voor Biotechnologie, Vrije Universiteit Brussel, Paardenstraat 65, B-1640 Sint-Genesius-Rode, Belgium
[2]Department of Organic Chemistry, Arrhenius Laboratory, Stockholm University, S-10691 Stockholm, Sweden
[3]Division of Organic and Bioorganic Chemistry, MBB, Scheele Laboratory, Karolinska Institutet, S-17177 Stockholm, Sweden

Correspondence: Stefan Loverix
E-mail: sloverix@vub.ac.be

**Keywords:** Catalysis; Mechanism; Ribonuclease; Thio-effect

Received: **15 March 2000**
Revisions requested: **5 April 2000**
Revisions received: **7 June 2000**
Accepted: **9 June 2000**

Published: **1 August 2000**

**Chemistry & Biology** 2000, **7**:651–658

1074-5521/00/$ – see front matter

PII: S1074-5521(00)00005-3

## Introduction

Ribonucleases (RNases) are a class of enzymes that cleave the phosphodiester bonds in RNA [1]. Their efficiency as catalysts is mirrored by an estimated $10^{15}$ increase in reaction rate ($(k_{uncat}/(k_{cat}/K_m))$ [2]. The catalyzed reaction is a transphosphorylation yielding a 2′,3′-cyclophosphate. This cyclic intermediate is hydrolyzed by a water molecule to a 3′-phosphate in a separate step which is the reversal of the transphosphorylation [3]. The transphosphorylation consists of a nucleophilic in-line inversion displacement at the phosphorus atom of the 5′-leaving group by the entering 2′-oxygen [4].

The classical RNase mechanism is thought to be concerted [5], with a trigonal bipyramidal phosphorane (TBP) structure along the reaction pathway, implying a base and an acid located on either side of the scissile bond (Figure 1A). However, the actual character of the TBP phosphorane structure, including its protonation state and whether it is a transition state or a true intermediate, has been an issue of considerable debate over the years for most RNases. Many questions regarding the microscopic details of the catalyzed reactions, including catalytic proton transfer steps, remain unresolved. Accordingly, a number of proposals for the TBP phoshorane structure is found in the literature. The classical acid–base mechanism [6,7] as illustrated in Figure 1A involves a monoanionic phosphorane. In this TBP structure, the nonbridging oxygens are not protonated and the catalytic acid and base interact exclusively with the apical oxygens in a concerted fashion. Triester-like mechanisms are characterized by early proton transfer to a nonbridging oxygen rendering the phosphate neutral, which facilitates nucleophilic attack by the 2′-alkoxide. In the Breslow mechanism [8] this proton comes from the catalytic acid (Figure 1B, right route). In an internal proton transfer mechanism [9,10], the proton comes from the 2′-OH group (Figure 1B, left route). Either way, the result is a monoanionic phosphorane. The likelihood of

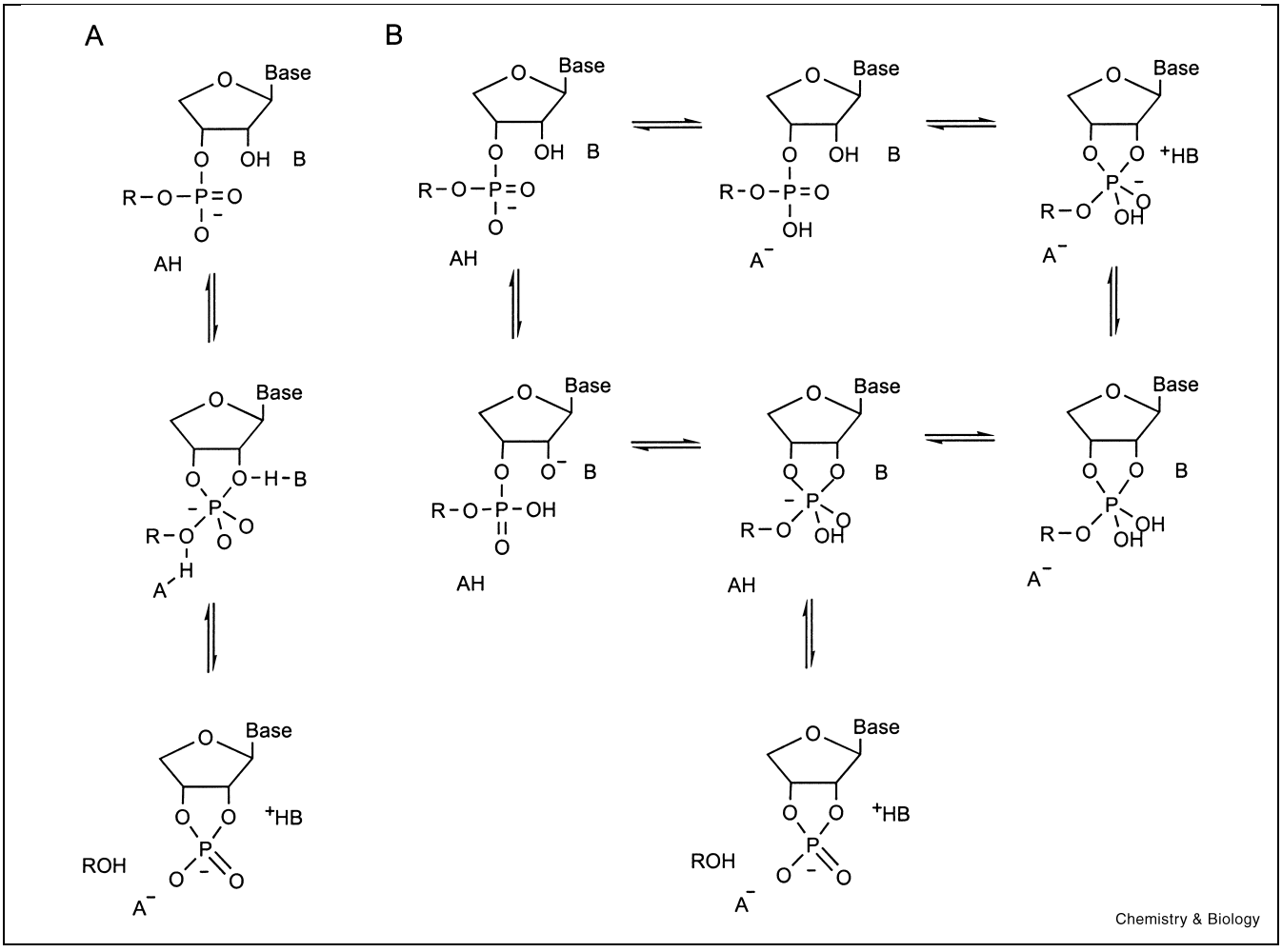


**Figure 1.** Microscopic events in RNase catalyzed phosphoryl transfer for classical concerted acid/base **(A)** versus triester-like **(B)** mechanisms. Triester-like mechanisms are characterized by protonation of a nonbridging oxygen, prior to attack by the 2′-nucleophile. In the Breslow-like mechanism (right route) this proton is donated by the catalytic acid. In the internal proton transfer mechanism (left route) the proton originates from the 2′-OH group.

a dianionic phosphorane, resulting from nucleophilic attack of the negatively charged 2′-alkoxide on the negatively charged phosphate, emerged from a computational study [9]. Such a TBP structure requires early proton transfer from the 2′-OH to the catalytic base. The relevance of a neutral phosphorane, with protonation of both nonbridging oxygens, has been established from an ab initio quantum chemical study [11].

RNase A (EC 3.1.27.5), one of the most thoroughly investigated enzymes (see review by Raines [12] for references), has historically been the model enzyme of choice to analyze phosphoryl transfer on phosphodiesters. RNase A is the representative of a homologous superfamily of vertebrate RNases [13]. A separate family of guanine-specific microbial RNases evolved to catalyze the same chemistry [14,15]. RNase $T_1$ (EC 3.1.27.3) from the slime mold *Aspergillus oryzae* and barnase from *Bacillus amyloliquefaciens* are the best known members of this microbial family. In the last decade, protein engineering [16] and X-ray crystallography [17] have revolutionized our knowledge of the structure–function relation of RNase $T_1$. It has been established that Tyr38, His40, Glu58, His92, and Phe100 are involved in the catalysis of RNA degradation. During cyclization, Glu58 and His92 serve as the catalytic base and acid, respectively [18,19]. It is currently believed that the protonated His40 imidazole engages the 2′-OH in a cooperative hydrogen bond with Glu58 (His40-$N_\varepsilon^+$H···O2′-H···$O_\varepsilon^-$-Glu58) to activate the nucleophile [20,21].

Whereas numerous experimental data point to a concerted acid–base mechanism for RNase A [22], the actual character of the transition state of the RNase $T_1$-catalyzed reaction remains unclear. The classical mechanism (Figure 1A)

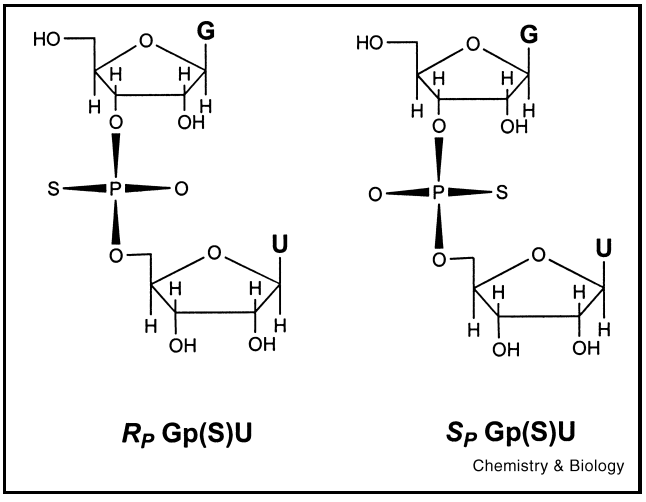


**Figure 2.** The diastereomers resulting from thio-substitution of a nonbridging oxygen in the model substrate GpU.

and the triester-like mechanism (Figure 1B) differ essentially in the protonation state of the nonbridging oxygens during transition state formation. We set out to analyze the catalytic interactions of RNase $T_1$ with these nonbridging oxygens. Therefore, we substituted the nonbridging oxygens of the phosphate by sulfur and analyzed the effects of these thio-substitutions on the kinetics of RNase $T_1$. Internucleotidic phosphorothioate diastereomers ($R_P$,$S_P$) resulting from substitutions of one nonbridging phosphoryl oxygen with sulfur (Figure 2) are common tools to investigate reaction stereochemistry [23], protein–nucleic acid interactions [24] or the role of metal ions in phosphoryl transfer [25]. The stereochemical course of RNase $T_1$ action, for example, has been established using the $R_P$ diastereomer of cyclic guanosine 2′,3′-phosphorothioate [26].

In a previous study, we used $R_P$ phosphorothioate RNA to probe the intermolecular interactions of RNase $T_1$ with the nonbridging *pro*-$R_P$ oxygen of the phosphodiester linkage during catalysis [27]. The method rested on the use of the $R_P$ diastereomer of guanylyl 3′,5′-uridine phosphorothioate ($R_P$ Gp(S)U), an optically pure phosphorothioate analogue of the dinucleoside phosphate GpU in which the *pro*-$R_P$ oxygen is replaced by sulfur (Figure 2). GpU was chosen as the parent dinucleoside phosphate substrate because its enzymic turnover is limited by the rate of bond making and breaking [28]. This is important because no mechanistic conclusion can be drawn from kinetic thio-effects if substrate association or product dissociation is rate-limiting. Since the uncatalyzed transphosphorylations of RNA and phosphorothioate RNA proceed with similar rates [29], any observed thio-effect on the catalyzed reactions reflects a change in the intermolecular interactions between the enzyme and the substrate in the transition state [30–32]. To confine these changes to a particular part of the active site, $R_P$ thio-effects were measured for wild type enzyme and a number of active site mutants (Table 1). This study revealed a catalytic hydrogen bond between Tyr38-$O_\eta$H and the *pro*-$R_P$ oxygen of the phosphate [27].

**Table 1**

The $S_P$ thio-effect on catalysis versus active site mutations.

| | GpU | | $S_P$ Gp(S)U | | Thio-effect[a] | Coupling[c] |
|---|---|---|---|---|---|---|
| | $k_{cat}/K_m$ ($mM^{-1}$ $s^{-1}$) | $\Delta G^b$ (kcal/mol) | $k_{cat}/K_m$ ($M^{-1}$ $s^{-1}$) | $\Delta G^b$ (kcal/mol) | | $\Delta\Delta G$ (kcal/mol) |
| Wild type | 1 000 | – | 11.3 | – | 88 500 | – |
| Tyr38Phe | 15.1 | 2.56 | 0.458 | 1.96 | 33 000 | 0.6 ± 0.2 |
| His40Ala | 0.153 | 5.38 | ND | ND | ND | ND |
| Glu58Ala | 27.40 | 2.20 | 7520 | −3.98 | 3.6 | 6.2 ± 0.2 |
| His92Gln | 0.117 | 5.54 | ND | ND | ND | ND |
| Phe100Ala | 1.38 | 4.03 | 8.65 | 0.17 | 160 | 3.9 ± 0.3 |

The $R_P$ thio-effect on catalysis versus active site mutations.

| | GpU | | $R_P$ Gp(S)U | | Thio-effect[a] | Coupling[c] |
|---|---|---|---|---|---|---|
| | $k_{cat}/K_m$ ($mM^{-1}$ $s^{-1}$) | $\Delta G^b$ (kcal/mol) | $k_{cat}/K_m$ ($mM^{-1}$ $s^{-1}$) | $\Delta G^b$ (kcal/mol) | | $\Delta\Delta G$ (kcal/mol) |
| Wild type | 1 000 | – | 665 | – | 1.50 | – |
| Tyr38Phe | 15.1 | 2.56 | 210 | 0.70 | 0.072 | 1.86 ± 0.13 |
| His40Ala | 0.153 | 5.38 | 0.029 | 6.15 | 5.33 | −0.77 ± 0.07 |
| Glu58Ala | 27.40 | 2.20 | 5.35 | 2.95 | 5.12 | −0.75 ± 0.07 |
| His92Gln | 0.117 | 5.54 | 0.028 | 6.17 | 4.21 | −0.63 ± 0.09 |
| Phe100Ala | 1.38 | 4.03 | 0.508 | 4.39 | 4.29 | −0.36 ± 0.07 |

ND: not determined due to very low activity.

[a]The thio-effect is defined as $(k_{cat}/K_m)^{phosphate}/(k_{cat}/K_m)^{phosphorothioate}$.

[b]Apparent interaction free energy between the deleted side chain and the substrate in ES‡, as calculated from the ratio of the $k_{cat}/K_m$ values of wild type enzyme and the mutant under investigation [44].

[c]Energetic coupling between the mutation under investigation and the substrate's thio-substitution. Values have been calculated from the difference in apparent interaction energy of a particular side chain with GpU and Gp(S)U, respectively.

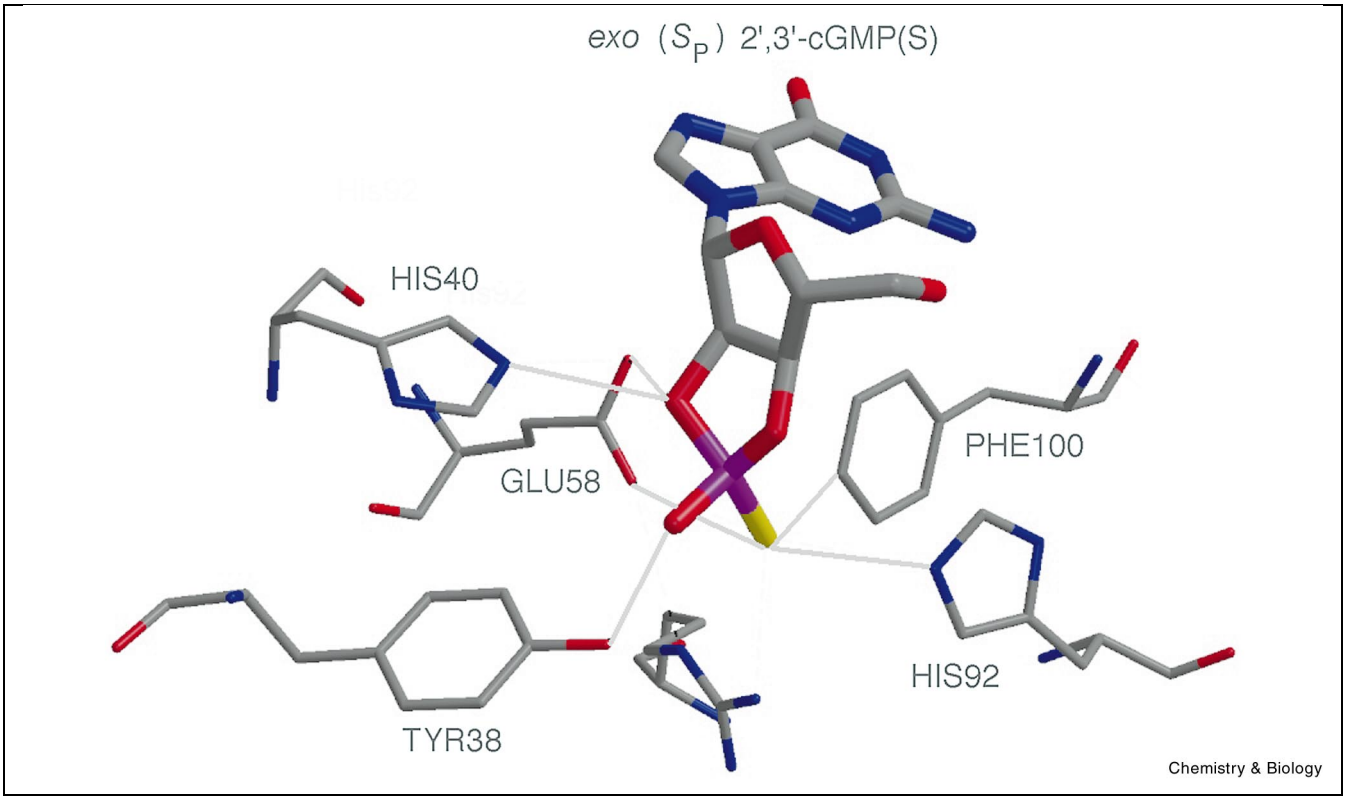


**Figure 3.** The active site of RNase $T_1$ in complex with *exo* ($S_P$) 2′,3′-cGMP(S), the product of the transphosphorylation of $S_P$ Gp(S)U. Possible hydrogen bonds are represented by gray lines. Nitrogen, oxygen, sulfur and phosphorus are represented in blue, red, yellow and magenta, respectively.

In the present study, we analyzed the kinetics of $S_P$ Gp(S)U for wild type enzyme and a number of mutants. We found that the thio-effect on the *pro*-$S_P$ position is coupled with the Glu58Ala mutation, indicating that RNase $T_1$ follows a triester-like mechanism that involves the Glu58-catalyzed protonation of the *pro*-$S_P$ oxygen.

## Results and discussion

### The large $S_P$ thio-effect is coupled to mutations at Glu58 and Phe100

First, we measured the kinetics of wild type RNase $T_1$ for the $S_P$ thio-substituted analogue of the dinucleoside phosphate GpU. We found that $S_P$ Gp(S)U is a very poor substrate for wild type RNase $T_1$ (Table 1). Its second-order rate constant ($k_{cat}/K_M$) is $9\times10^4$-fold and $6\times10^4$-fold smaller than that for GpU and $R_P$ Gp(S)U, respectively [27]. The equilibrium dissociation constant of the enzyme–substrate complex ($K_S$ equals $K_M$ in each case) is not dependent on thio-substitution, indicating that the enzyme's stereoselectivity is solely due to weakened binding of the $S_P$ Gp(S)U transition state. It appears that the substitution of the *pro*-$S_P$ oxygen by sulfur prevents an optimal spatial and/or electronic complementarity with the active site, since thio-substitution does not affect the uncatalyzed reaction. RNase $T_1$ shares this stereoselective behavior with snake venom phosphodiesterase, but not with RNase A or RNase $T_2$ [33].

To probe the intermolecular interactions of the enzyme with the nonbridging *pro*-$S_P$ oxygen that brings about this stereoselectivity of RNase $T_1$ we confined the $S_P$ thio-effect to a particular part of the enzyme active site. Therefore, we compared the $S_P$ thio-effect for wild type enzyme with the thio-effects measured for a number of active site mutants (Table 1). Changes in the thio-effect upon deletion of a particular side chain are indicative of direct and/or indirect intermolecular interactions between the deleted side chain and the *pro*-$S_P$ oxygen atom in the reference ES$^‡$ complex [27,30–32]. The energetic coupling between a particular mutation and the thio-substitution can be expressed quantitatively as the difference in apparent interaction free energy of the side chain under investigation with GpU and $S_P$ Gp(S)U, respectively ($\Delta\Delta G$ in Table 1). This type of analysis by means of single mutant enzymes and modified substrates is conceptually identical to the use of double mutants to study intra- or intermolecular interactions in proteins [34]. We found that the effects of the Glu58Ala and Phe100Ala mutations on the turnover rate change considerably upon $S_P$ thio-substitution. Such effect is not observed for Tyr38Phe RNase $T_1$. The resid-

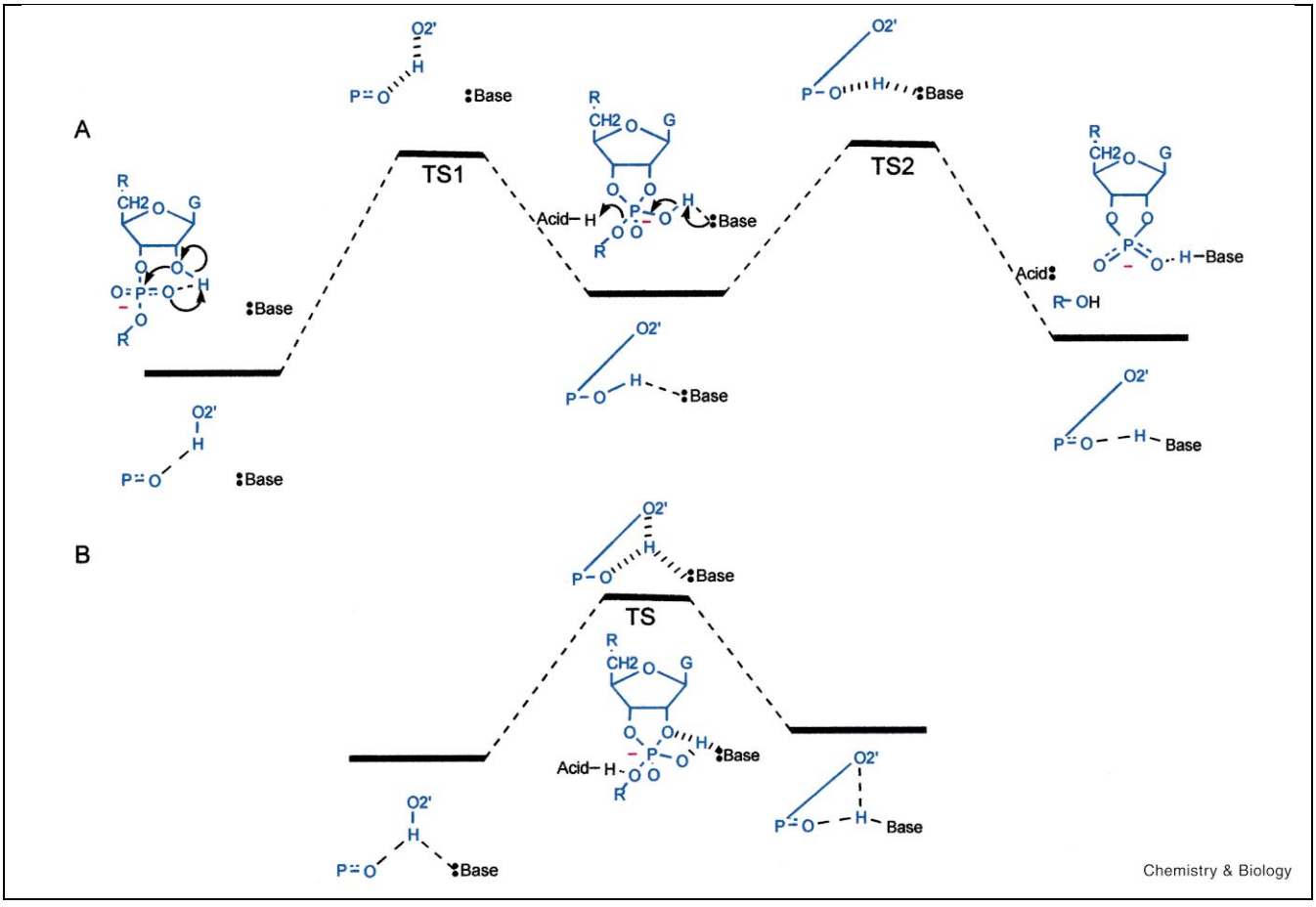


**Figure 4.** Hypothetical reaction coordinates for a triester-like mechanism involving internal proton transfer. Proton transfer in the transition states is depicted by dashed lines. For a sequential mechanism (reaction coordinate **(A)**, a first transition state TS1 involving proton transfer from the nucleophile to a nonbridging oxygen is followed by a second transition state TS2 involving abstraction of this proton by the catalytic base and concomitant expulsion of the leaving group. The three-centered hydrogen bond concept merges both events into a single transition state TS along the reaction coordinate **(B)**.

ual activities of His40Ala and His92Gln RNase $T_1$ for $S_P$ Gp(S)U were below our detection limit. The large coupling between the $S_P$ thio-effect and the Glu58Ala and Phe100Ala mutations indicate that the suboptimal spatial and/or electronic fit between the active site and the sulfur is caused by the side chains of Glu58 and Phe100. These kinetic observations are consistent with crystallographic data on RNase $T_1$ in complex with $S_P$ 2′,3′-cGMP(S), the product of the transphosphorylation of $S_P$ Gp(S)U (Figure 3) [35]. In this complex, Glu58 and Phe100 are located at the requisite side of the cyclophosphate to interact with the *pro*-$S_P$ oxygen in the transition state.

The remarkable coupling (6.2 kcal/mol, Table 1) between the $S_P$ thio-substitution and the Glu58Ala mutation reflects an interaction between the *pro*-$S_P$ oxygen of the substrate and the Glu58 side chain that is particularly relevant for the transition state. The Glu58Ala mutation reduces $k_{cat}/K_m$ for the reference substrate GpU 36-fold. Surprisingly, the same mutation improves $k_{cat}/K_m$ for $S_P$ Gp(S)U 660-fold (Table 1). Glu58Ala RNase $T_1$ is thus a moderate catalyst for $S_P$ phosphorothioate RNA, whereas the wild type enzyme is severely impaired for this substrate. All kinetic data can conveniently be explained by a short hydrogen bond between one of the carboxylate oxygens of Glu58 and the *pro*-$S_p$ phosphate oxygen upon catalysis. This short hydrogen bond turns into a repulsive contact when the *pro*-$S_p$ phosphate oxygen is replaced by sulfur, likely through steric hindrance or through reduced proton affinity for sulfur as compared to oxygen. We find that removal of the glutamate side chain eliminates the repulsive interaction with sulfur, thus improving the affinity of the enzyme for the transition state of $S_P$ thio-substituted substrates.

Like Glu58, deletion of the Phe100 side chain decreases $k_{cat}/K_m$ for GpU but increases $k_{cat}/K_m$ for $S_P$ Gp(S)U, resulting in a coupling energy of about 3.9 kcal/mol (Table

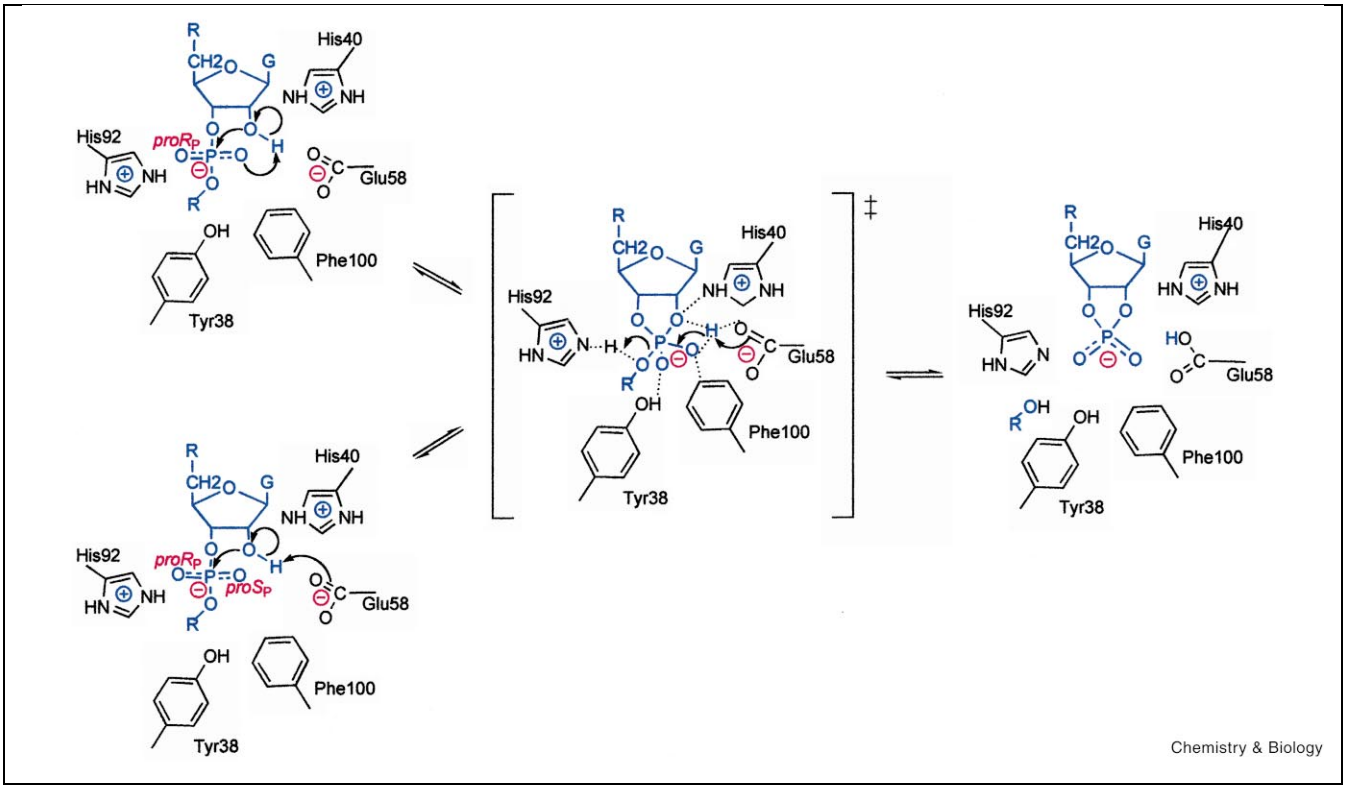


**Figure 5.** Function of the active site residues in the RNase $T_1$-catalyzed transphosphorylation of RNA via a three-centered hydrogen bond mechanism.

1). This coupling mirrors a stabilizing interaction between the Phe100 aromatic ring and the *pro*-$S_P$ oxygen during catalysis. Apparently, this interaction turns into a repulsive contact when the *pro*-$S_P$ oxygen is replaced by sulfur. In the complex of RNase $T_1$ with $S_P$ 2′,3′-cGMP(S), the aromatic ring of Phe100 is in close van der Waals contact (3.2 Å) with the sulfur (Figure 3). Thio-substitution may generate a steric clash between the TBP transition state and Phe100. Indeed, a sulfur atom on phosphorus projects outward about 0.8 Å more than an oxygen atom [36]. Accordingly, removal of the aromatic ring in the Phe100Ala mutant allows for a more convenient accommodation of the sulfur atom in the transition state complex.

### A triester-like mechanism involving internal proton transfer

So far, it was believed that RNase $T_1$ follows the classical concerted acid–base mechanism (Figure 1A). However, recapitulation of older data on RNase $T_1$ [26] and analysis of the present results support the likelihood of a triester-like mechanism. Triester-like mechanisms (Figure 1B) depend on the protonation of one of the nonbridging phosphoryl oxygens, rendering the transition state more like a phosphotriester, which is $10^3$ to $10^5$ times more reactive than the corresponding phosphodiester [37]. An important piece of evidence indicating that RNase $T_1$ follows such a triester-like mechanism results from the observation that substitution of the *pro*-$S_P$ oxygen by sulfur reduces the turnover of the model substrate GpU $10^5$-fold (Table 1). Such a large thio-effect is not observed when the *pro*-$R_P$ oxygen is replaced by sulfur [27]. Because sulfur has a much lower affinity for protons than oxygen, a large thio-effect would be predicted for at least one of the thio-isomers if the enzyme follows a triester-like mechanism [7]. The fact that RNase $T_1$ exhibits an exclusive $S_P$ thio-effect reflects the protonation of the *pro*-$S_P$ oxygen during the rate-limiting step. The *pro*-$R_P$ oxygen appears to remain unprotonated. A second piece of evidence for a triester-like mechanism comes from the observation that the general base Glu58 interacts with the *pro*-$S_P$ oxygen in the rate-limiting step. This observation is inconsistent with the classical acid–base mechanism [6,7] as in Figure 1A. In such a mechanism, the catalytic base interacts exclusively with the apical 2′-oxygen.

Various triester-like mechanisms found in the literature differ essentially in the origin of the (catalytic) proton that is initially transferred to a nonbridging oxygen. In a Breslow-like mechanism [8] (right route in Figure 1B) the proton comes from the catalytic acid, whereas the proton comes from the 2′-OH group in an internal proton transfer mechanism [9,10] (left route in Figure 1B). Structural lim-

itations of the RNase $T_1$ active site render the substrate's 2′-OH group as the most probable source of the catalytic proton that has to be transferred to the *pro*-$S_P$ nonbridging oxygen. Our finding that Glu58, being the catalytic base of RNase $T_1$ [18], interacts with the *pro*-$S_P$ oxygen in the transition state strongly suggests that Glu58 catalyzes the protonation of this nonbridging oxygen. Phe100 may contribute to this protonation step by tailoring the local dielectric environment [38]. All these considerations point to a triester-like internal proton transfer mechanism as depicted in Figure 1B (left route) and Figure 4A. After the formation of the TBP structure, the catalytic proton is abstracted from the *pro*-$S_P$ nonbridging oxygen by the catalytic base Glu58, leading to the expulsion of the leaving group.

The marginal decrease in $k_{cat}$ (20-fold) upon deletion of the Glu58 carboxylate ([18]; see also Table 1) seems to minimize the role of this residue as a general base and as a catalytic device to protonate the *pro*-$S_P$ oxygen. It has been shown however, that the unprotonated His40 takes over the role of general base if Glu58 is replaced by alanine [18]. This mutant uses two histidines as acid–base pair and may well function according to a more classical mechanism, as is the case for RNase A. Alternatively, His40 may abstract the proton from the 2′-OH group via a water molecule that is found in the cavity created by the Glu58Ala mutation [39]. This water molecule may also interact catalytically with the *pro*-$S_P$ oxygen, thus compensating largely for the Glu58Ala mutation.

### A three-centered hydrogen bond for concerted phosphoryl transfer

In triester-like mechanisms, nucleophile activation, nucleophilic attack and leaving group expulsion are more or less separate events resulting in more or less stable intermediates on the reaction coordinate (Figure 4A). The presence of such intermediates has never been established, neither in RNase $T_1$, nor in RNase A or any other RNase. Building on this consideration, we put forward a concerted alternative (Figure 4B) that relies on a three-centered hydrogen bond in the transition state. In this three-centered hydrogen bond, the nucleophilic 2′-oxygen, the *pro*-$S_P$ oxygen and the catalytic base cluster around the proton that has to be abstracted from the 2′-OH group. We postulate that the proton is bound symmetrically in this three-centered configuration in the transition state. If the hydrogen bonds are short and the proton is symmetrically located in the plane of the three donor/acceptor atoms, the barrier to proton tunneling may be relatively low [40]. Simultaneous proton transfer from 2′-OH towards the *pro*-$S_P$ oxygen and the catalytic base could allow nucleophilic attack on an activated phosphate and general base catalysis to occur in the same transition state (Figure 4B). In a concerted mechanism, formation of the three-centered hydrogen bond accompanies the expulsion–protonation of the 5′-leaving group. This new view on the mechanism of RNase $T_1$ leads to an almost complete picture of the intermolecular interactions between the enzyme and the transition state of the reaction (Figure 5). The interactions of Arg77 with the transition state remain obscure because the function of this residue can not be probed by site-directed mutagenesis. The guanidinium group of this residue has a unique structural role that can not be fulfilled by any other natural amino acid.

## Significance

**The microscopic events of the RNase catalyzed phosphoryl transfer reactions are still a matter of debate. Internucleotidic phosphorothioate diastereomers ($R_P$,$S_P$) resulting from substitutions of one nonbridging phosphoryl oxygen with sulfur have been used as diagnostic tools to discriminate between the classical concerted acid–base mechanism or a more sequential triester-like mechanism. In this work, we combined this type of site-specific substrate modification with site-directed mutagenesis in RNase $T_1$, the best known representative of a large family of microbial RNases. We found that the large kinetic effect associated with the thio-substitution of the nonbridging *pro*-$S_P$ oxygen (the $S_P$ thio-effect) is coupled to the presence of the general base Glu58 of RNase $T_1$. These data indicate that RNase $T_1$ follows a triester-like mechanism featuring internal proton transfer catalyzed by the general base Glu58. Our new proposal implies a three-centered hydrogen bond that allows nucleophilic attack on an activated phosphate to occur simultaneously with general base catalysis, ensuring concerted phosphoryl transfer in a triester-like mechanism. Three-centered hydrogen bonds are widely recognized in protein structure and are believed to be major players in dynamic processes like ligand binding and protein hydration. Because catalysis is a dynamic process as well, three-centered hydrogen bonds may be more relevant to enzyme–substrate interactions than recognized so far.**

## Materials and methods

### *Materials*

The 3′,5′-dinucleoside phosphate substrate GpU and buffer substances were from Sigma. The preparation of wild type enzyme and all single mutants has been reported previously [18,38]. All enzymes were purified to homogeneity following standard procedures [41]. Chemical synthesis of guanylyl 3′,5′-uridine phosphorothioate (Gp(S)U) was performed as described [42]. The isomers were separated and purified by reversed phase HPLC (Hypersil ODS, RP-C18, 5 μm) using a linear gradient from 0.1 M triethylammonium acetate buffer (pH 6.5) to the same buffer containing 15% acetonitrile.

### *Kinetic procedures*

The steady-state kinetic parameters were determined from initial rate experiments where first-order kinetics were observed at all times. The concentrations of GpU and $S_P$ Gp(S)U were measured spectroscopically at 280 nm using the same extinction coefficient equal to 10 600 $M^{-1}$ $cm^{-1}$. The transphosphorylation of GpU was followed spectroscopically at 280 nm, where $\Delta\varepsilon = 840$ $M^{-1}$ $cm^{-1}$. The reaction progress of Gp(S)U transphosphorylation was monitored via calibrated reversed phase HPLC analysis (Hypersil ODS, RP-C18, 3 μm). The column was equilibrated with formic acid–sodium formate buffer (0.045:0.015

M) containing 0.1 M tetramethylammonium chloride. The substrate $S_P$ Gp(S)U was separated from the product *exo* ($S_P$) 2′,3′-cGMP(S) using a gradient of 7–40% (v/v) acetonitrile as the eluant. Enzyme and substrate were mixed and incubated at 35°C, pH 6.0. Aliquots taken at different time intervals were quantified after detection at 256 nm by peak integration [29]. The rates of the linear decay of substrate at various substrate concentrations were calculated by linear regression analysis of the experimental data. Values for $k_{cat}$ and $K_M$ were obtained by fitting plots of rate versus substrate concentration using the program Origin™ [43].

## Acknowledgements

This work was supported by the Vlaams Interuniversitair Instituut voor Biotechnologie, the Fonds voor Wetenschappelijk Onderzoek-Vlaanderen, and a scolarship to S.L. from the Vlaams Instituut voor de bevordering van het Wetenschappelijk-Technologisch Onderzoek in de Industrie.

## References

1. D'Alessio, G. & Riordan, J.F. (1997). *RNases: Structures and Functions*, (1st edn.), Academic Press, New York.
2. Thompson, J.E., Kutateladze, T.G., Schuster, M.C., Venegas, F.D., Messmore, J.M. & Raines, R.T. (1995). Limits to Catalysis by Ribonuclease A. *Bioorg. Chem.* **23**, 471–481.
3. Loverix, S., Laus, G., Martins, J.C., Wyns, L. & Steyaert, J. (1998). Reconsidering the energetics of ribonuclease catalysed RNA hydrolysis. *Eur. J. Biochem.* **257**, 286–290.
4. Eckstein, F., Saenger, W. & Suck, D. (1972). Stereochemistry of the transesterification step of pancreatic ribonuclease. *Biochem. Biophys. Res. Commun.* **46**, 964–971.
5. Findlay, D., Herries, D.G., Mathias, A.P., Rabin, B.R. & Ross, C.A. (1961). The active site and mechanism of action of bovine pancreatic ribonuclease. *Nature* **190**, 781–784.
6. Thompson, J.E. & Raines, R.T. (1994). Value of general acid–base catalysis to ribonuclease A. *J. Am. Chem. Soc.* **116**, 5467–5468.
7. Herschlag, D. (1994). Ribonuclease revisited: catalysis via the classical general acid–base mechanism or a triester-like mechanism? *J. Am. Chem. Soc.* **116**, 11631–11635.
8. Breslow, R. & Chapman, W.H.Jr. (1996). On the mechanism of action of ribonuclease A: Relevance of enzymatic studies with a *p*-nitrophenylphosphate ester and a thiophosphate ester. *Proc. Natl. Acad. Sci. USA* **93**, 10018–10021.
9. Glennon, T.M. & Warshel, A. (1998). Energetics of the catalytic reaction of ribonuclease A: A computational study of alternative mechanisms. *J. Am. Chem. Soc.* **120**, 10234–10247.
10. Wladkowski, B.D., Svensson, L.A., Sjolin, L., Ladner, J.E. & Gilliland, G.L. (1998). Structure (1.3 Å) and charge states of a ribonuclease A–uridine vanadate complex: implications for the phosphate ester hydrolysis mechanism. *J. Am. Chem. Soc.* **120**, 5488–5498.
11. Wladkowski, B.D., Krauss, M. & Stevens, W.J. (1995). Transphosphorylation catalyzed by ribonuclease A: computational study using ab initio effective fragment potentials. *J. Am. Chem. Soc.* **117**, 10537–10545.
12. Raines, R.T. (1998). Ribonuclease A. *Chem. Rev.* **98**, 1045–1066.
13. Beintema, J.J. (1998). Introduction: the ribonuclease A superfamily. *Cell Mol. Life Sci.* **54**, 763–765.
14. Mauguen, Y. et al. (1982). Molecular structure of a new family of ribonucleases. *Nature* **297**, 162–164.
15. Hill, C. et al. (1983). The structural and sequence homology of a family of microbial ribonucleases. *Trends Biochem. Sci.* **8**, 364–369.
16. Steyaert, J. (1997). A decade of protein engineering on ribonuclease $T_1$-atomic dissection of the enzyme–substrate interactions. *Eur. J. Biochem.* **247**, 1–11.
17. Heinemann, U. & Hahn, U. (1989). Structural and functional studies of ribonuclease $T_1$. In *Protein–Nucleic Acid Interactions*. (Saenger, W. & Heinemann, U., eds.), pp. 111–141, MacMillan, London.
18. Steyaert, J., Hallenga, K., Wyns, L. & Stanssens, P. (1990). Histidine-40 of ribonuclease $T_1$ acts as base catalyst when the true catalytic base, glutamic acid-58, is replaced by alanine. *Biochemistry* **29**, 9064–9072.
19. De Vos, S., Doumen, J., Langhorst, U. & Steyaert, J. (1998). Dissecting histidine interactions of ribonuclease $T_1$ with asparagine and glutamine replacements: analysis of double mutant cycles at one position. *J. Mol. Biol.* **275**, 651–661.
20. Heydenreich, A. et al. (1993). The complex between ribonuclease $T_1$ and 3′GMP suggests geometry of enzymic reaction path. An X-ray study. *Eur. J. Biochem.* **218**, 1005–1012.
21. Steyaert, J. & Wyns, L. (1993). Functional interactions among the His40, Glu58 and His92 catalysts of ribonuclease $T_1$ as studied by double and triple mutants. *J. Mol. Biol.* **229**, 770–781.
22. Silverman, R.B. (2000). Phosphorylations: transfers of phosphate esters to water or other acceptors. In *The Organic Chemistry of Enzyme-catalyzed Reactions.* pp. 76–90, Academic Press, London.
23. Eckstein, F. (1985). Nucleoside phosphorothioates. *Annu. Rev. Biochem.* **54**, 367–402.
24. Milligan, J.F. & Uhlenbeck, O.C. (1989). Determination of RNA–protein contacts using thiophosphate substitutions. *Biochemistry* **28**, 2849–2855.
25. Warnecke, J.M., Held, R., Busch, S. & Hartmann, R.K. (1999). Role of metal ions in the hydrolysis reaction catalyzed by RNase P RNA from *Bacillus subtilis*. *J. Mol. Biol.* **290**, 433–445.
26. Eckstein, F., Schulz, H.H., Rüterjans, H., Haar, W. & Maurer, W. (1972). Stereochemistry of the transesterification step of ribonuclease $T_1$. *Biochemistry* **11**, 3507–3512.
27. Loverix, S., Winqvist, A., Strömberg, R. & Steyaert, J. (1998). An engineered ribonuclease preferring phosphorothioate RNA. *Nat. Struct. Biol.* **5**, 365–368.
28. Steyaert, J., Wyns, L. & Stanssens, P. (1991). Subsite interactions of ribonuclease $T_1$: viscosity effects indicate that the rate-limiting step of GpN transesterification depends on the nature of N. *Biochemistry* **30**, 8661–8665.
29. Oivanen, M., Ora, M., Almer, H., Strömberg, R. & Lönnberg, H. (1995). Hydrolytic reactions of the diastereomeric phosphoromonothioate analogs of uridylyl(3′,5′)uridine: kinetics and mechanisms for desulfurization, phosphoester hydrolysis, and transesterification to the 2′,5′-isomers. *J. Org. Chem.* **60**, 5620–5627.
30. Hondal, R.J., Bruzik, K.S., Zhao, Z. & Tsai, M.D. (1997). Mechanism of phosphatidylinositol-phospholipase c. 2. reversal of a thio effect by site-directed mutagenesis. *J. Am. Chem. Soc.* **119**, 5477–5478.
31. Admiraal, S.J. et al. (1999). Nucleophilic activation by positioning in phosphoryl transfer catalyzed by nucleoside diphosphate kinase. *Biochemistry* **38**, 4701–4711.
32. Zhang, Y.L. et al. (1999). Impaired transition state complementarity in the hydrolysis of *O*-arylphosphorothioates by protein-tyrosine phosphatases. *Biochemistry* **38**, 12111–12123.
33. Burgers, P.M.J. & Eckstein, F. (1979). Diastereomers of 5′-*O*-adenosyl 3′-*O*-uridyl phosphorothioate: chemical synthesis and enzymatic properties. *Biochemistry* **18**, 592–596.
34. Horovitz, A. (1996). Double-mutant cycles: a powerful tool for analyzing protein structure and function. *Fold. Des.* **1**, 121–126.
35. Zegers, I. et al. (1998). Hydrolysis of a slow cyclic thiophosphate substrate of RNase $T_1$ analyzed by time-resolved crystallography. *Nat. Struct. Biol.* **5**, 280–283.
36. Saenger, W. (1984). *Principles of Nucleic Acid Structure* (1st edn.). Springer-Verlag, New York.
37. Chandler, A.J., Hollfelder, F., Kirby, A.J., O'Carroll, F. & Stromberg, R. (1994). Models for enzyme-catalysed phosphate transfer: comparisons of reactivity towards a neighbouring hydroxy group for phosphodiester anions and acids. general base catalysis of the cyslisation of a hydroxyalkyl phosphate triester. *J. Chem. Soc. Perkin Trans. 2* 327–333.
38. Doumen, J., Gonciarz, M., Zegers, I., Loris, R., Wyns, L. & Steyaert, J. (1996). A catalytic function for the structurally conserved residue Phe 100 of ribonuclease $T_1$. *Protein Sci.* **5**, 1523–1530.
39. Pletinckx, J., Steyaert, J., Zegers, I., Choe, H.W., Heinemann, U. & Wyns, L. (1994). Crystallographic study of Glu58Ala RNase $T_1 \times 2'$-guanosine monophosphate at 1.9-Å resolution. *Biochemistry* **33**, 1654–1662.
40. Jeffrey, G.A. & Saenger, W. (1991). *Hydrogen Bonding in Biological Structures* (1st edn.). Springer-Verlag, Berlin.
41. Mayr, L.M. & Schmid, F.X. (1993). A purification method for labile variants of ribonuclease $T_1$. *Protein Expr. Purif.* **4**, 52–58.
42. Almer, H., Stawinski, J., Strömberg, R. & Thelin, M. (1992). Synthesis of diribonucleoside phosphorothioates via stereospecific sulfurization of H-phosphonate diesters. *J. Org. Chem.* **57**, 6163–6169.
43. Microcal Software, I. (1991). Microcal™ Origin™.
44. Fersht, A.R. (1988). Relationships between apparent binding energies measured in site-directed mutagenesis experiments and energetics of binding and catalysis. *Biochemistry* **27**, 1577–1580.